A Field Panel/Finite Difference Method for Potential Unsteady Transonic Flow

M.H.L. Hounjet*
National Aerospace Laboratory NLR, Amsterdam, The Netherlands

A hybrid method for calculating time-linearized transonic potential flows is described. The method combines the advantages of finite difference and integral methods such that computation times are reduced to a level acceptable for routine flutter applications. The corresponding computer code FTRAN3 has been applied to several wing planforms. The results correlate satisfactorily with experimental data and results of other calculation methods.

Introduction

In the development of many modern airplanes flutter clearances are required in the transonic speed range. This implies a growing need for reliable oscillatory wing loads for many mixed subsonic-supersonic flow conditions to be calculated at an economical price.

For two-dimensional flow, several "time-integrating" finite difference methods have been developed successfully[1,2] which fulfill these requirements. For three-dimensional extensions,[3-6] however, the computational cost, which is proportional to $\mathcal{O}(N\times Ni)$, where N is the number of mesh points and Ni the number of successive iterations in time, seems to be too high for routine flutter applications.[7]

At NLR research was started some years ago in an attempt to lower the computational cost by using a "time-linearized," transonic, small-perturbation flow equation model solved by an "exact" integral method, a so-called field panel method, which had the following advantages: 1) substantial reduction of the number of mesh points, while also grid generation is facilitated; 2) strong reduction of the number of iterations Ni needed for convergence; and 3) satisfied "exact" radiation conditions. This research led to a successful two-dimensional field panel method[8,9] with the following disadvantages: 1) higher computational complexity and 2) computational cost proportional to $\mathcal{O}(N\times N\times Ni)$. For this reason, straightforward extension to three-dimensional flows, for which N increases by approximately one order of magnitude, would be hampered by the computational cost.

To lower the computational cost, further investigations for improvement were initiated at NLR.[9,10] Therefore, it was concluded that a combination of "time-linearized" finite difference and field panel methods would be preferable in terms of computational complexity and cost. The finite difference method was adopted to deal with the fast local variations of the flow variables in the immediate neighborhood of the wing, while the field panel method should describe the smoother variations at some distance away from the wing. Along this line a new method has been developed, encompassing a multigrid finite difference method which uses an integral method for the generation of radiation conditions at an artificial outer boundary not far from the wing. The corresponding computer code is called FTRAN3.

The present paper describes the method and presents results of three-dimensional applications. The computational cost of a routine run ($N=10{,}000$) is about four times the cost needed for an application of the well-known subsonic doublet-lattice method[11] using 200 boundary panels.

Outline of Present Method

The solution of the time-linearized, transonic potential flow problem is obtained by a mixture of two recent developments in transonic flow calculation methods: 1) multigrid iterative approach for fast convergence, and 2) integral methods which reduce the number of grid points and by which grid generation is facilitated.

The multigrid iterative approach can be considered as the approximation of the potential by a set of subpotentials characterized by a certain wavelength. Usually each subpotential is defined on a grid system with a characteristic mesh spacing. This approach has proved to yield very efficient solution methods.[15]

The integral method is based on the approximation of the potential by a set of functions satisfying the radiation conditions. By this it is possible to restrict the computational domain to the region where nonuniform compressibility effects are important.

The present combination is obtained after replacing the multigrid subpotential on the coarsest grid by the integral approximation and to approximate the total potential at the outer boundary by the integral approximation. The mathematical formulation of the method and the multigrid approach are described in the following sections.

Mathematical Formulations

The boundary-value problem that governs the unsteady, time-linearized, inviscid, transonic potential flow past a three-dimensional wing is shown in Fig. 1. Its formulation is well known and is recapitulated here. When Φ_0 and φ denote the mean steady and first harmonic components of the velocity potential, the time-linearized, full-potential equation operator $L(\varphi)$ is expressed by

$$L(\varphi)=\nabla\cdot(\rho^0\nabla\varphi+\rho^1\nabla\Phi_0)+ik\rho^1=0$$

where the mean steady and first harmonic densities ρ^0 and ρ^1 are defined by

$$\rho^0=[1+(\gamma-1)M^2(1-\nabla\Phi_0\cdot\nabla\Phi_0)/2]^{1/(\gamma-1)}$$

and

$$\rho^1=-\rho^0[ik\varphi+\nabla\Phi_0\cdot\nabla\varphi]/a_0^2$$

Presented as Paper 83-1690 at the AIAA 16th Fluid and Plasma Dynamics Conference, Danvers, Mass., July 12-14, 1983; received July 25, 1983; revision received April 30, 1984.

*Research Engineer, Department of Aeroelasticity, Division of Fluid Dynamics.

where a_0 is the mean steady speed of sound

$$a_0^2 = 1/M^2 + (\gamma - 1)(1 - \nabla\Phi_0 \cdot \nabla\Phi_0)/2$$

The boundary condition at the wing surface for tangential flow is

$$\varphi_N = f = \nabla\Phi_0 \cdot \nabla h + ikh$$

where the subscript N means differentiation along the outward normal at the wing surface and h is the first harmonic displacement of the wing. Cp^0 and Cp^1 denote the mean steady and the first harmonic component of the pressure coefficient which has been made dimensionless with the dynamic pressure, given by the expressions:

$$Cp^0 = -2(\rho^{0\gamma} - 1) \text{ and } Cp^1 = -2\rho^0[ik\varphi + \nabla\Phi_0 \cdot \nabla\varphi]$$

Furthermore, M is the freestream Mach number; k the reduced frequency; $k = \omega\ell/U$, where ℓ denotes the reference length and U the undisturbed flow speed; and γ the ratio of specific heats. The variables are all made dimensionless with ℓ and U.

The first harmonic of the velocity potential can be expressed by the differential-integral transform pair

$$m = H[\varphi] \tag{1}$$

$$\varphi = I[m] = I[H[\varphi]] \rightarrow I = H^{-1} \tag{2}$$

in which H denotes the classical differential operator for uniform subsonic flow

$$H[\varphi] = (1 - M^2)\varphi_{xx} + \varphi_{yy} + \varphi_{zz} - 2ikM^2\varphi_x + k^2M^2\varphi \tag{3}$$

and I the integral operator,

$$I[m] = \int_{-\infty}^{\infty}\int\int mE(x-u, y-v, z-w)\,du\,dv\,dw \tag{4}$$

where E satisfies the radiation conditions, and

$$H[E] = \delta(x)\delta(y)\delta(z) \tag{5}$$

The solution of E is

$$E(x,y,z) = \frac{\exp[ikM(Mx - r)/(1 - M^2)]}{-4\pi r} \tag{6}$$

where $r = [x^2 + (y^2 + z^2)(1 - M^2)]^{1/2}$.

Inside the wing and wake surface the potential may be continued freely. For example, choosing $\varphi = 0$ inside the volume V_C enclosed by the wing and wake surface C reduces the integral part in case $M = 0$ over it into the well-known surface integral

$$\int\int\int_{V_C} mE\,dV = -\int\int_C (\varphi E_N - \varphi_N E)\,dC \tag{7}$$

Substitution of Eq. (2) plus additional continuation into the field equation and boundary conditions at C, which are given in Fig. 1, changes the primary variable φ into the variable m. m represents a volume source distribution; and/or a surface source distribution; and/or a surface doublet distribution, depending on the additional continuation in V_C.

Next the infinite integration domain is restricted to a finite domain by introducing an artificial boundary A at a finite distance from C and neglecting $H[\varphi]$ outside A (except for the wake), or, in other words, supposing the fluid is uniformly compressible at and outside A.

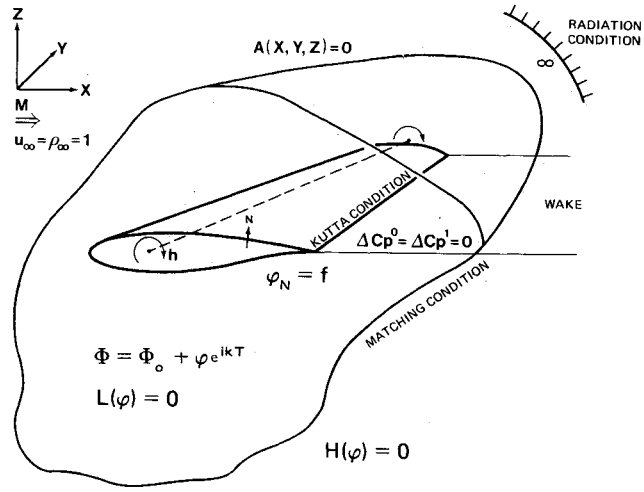

Fig. 1 Boundary-value problem.

Of course, this restriction introduces an error to which some observations can be made:

1) The error *cannot* be modeled by a series of multipoles located inside A, for that would give no contribution to $H[\varphi]$ outside A.

2) The error can be approximated by a series of eigensolutions of $H[f] = \lambda f$ satisfying radiation conditions ($\lambda \neq 0$).

3) This suggests exponential decay of the error.

4) A conservative estimate of the error involved is probably $\mathcal{O}(H[\varphi]_A)$. The aforementioned approach was used for two-dimensional cases.[8,9]

In the present approach φ is further approximated by a set of band-limited functions:

$$\varphi = \sum_{m=0}^{M} F_m[\varphi] = \sum_{m=0}^{M} \varphi_m = \sum_{m=0}^{N-1} \varphi_m + \sum_{m=N}^{M} \varphi_m$$

$$= I\left[H\left[\sum_{m=0}^{N-1} \varphi_m\right]\right] + \sum_{m=N}^{M} \varphi_m \tag{8}$$

and supposing

$$\varphi_m = 0 \text{ at } A, \quad m \geq N \tag{9}$$

where F is a band filter operator to be defined such that each φ_m has a smaller bandwidth (smaller minimum sample rate) than φ_{m+1} and also the integral transform is restricted to a smoother part of φ.

The assumption [Eq. (9)] is pursuant to the fact that the functional behavior of φ at A is supposed to be characterized by a relatively larger wavelength than φ at the wing.

Multigrid Method

The aforementioned boundary-value problem is solved by a multigrid procedure. For a discussion of multigrid methods see Ref. 12. Presently two levels are being used, i.e., $M = N = 1$. According to approximations (8) and (9), two types of grids are introduced: 1) a fine grid on which finite difference calculations take place for φ_1, and 2) a coarse grid on which integral (field panel) calculations are performed for φ_0.

The calculations are coupled by exchange of information between the fine and coarse grids. Interpolation of coarse to fine is performed by a so-called prolongation operator P. Transport from fine to coarse is performed by a restriction operator R. φ_0 is determined by the numerical band filter $P[R[\varphi]]$.

The present procedure consists of the following steps:

1) Calculation of defects on the fine grid,

$$d_f^n = L_f\varphi^n$$

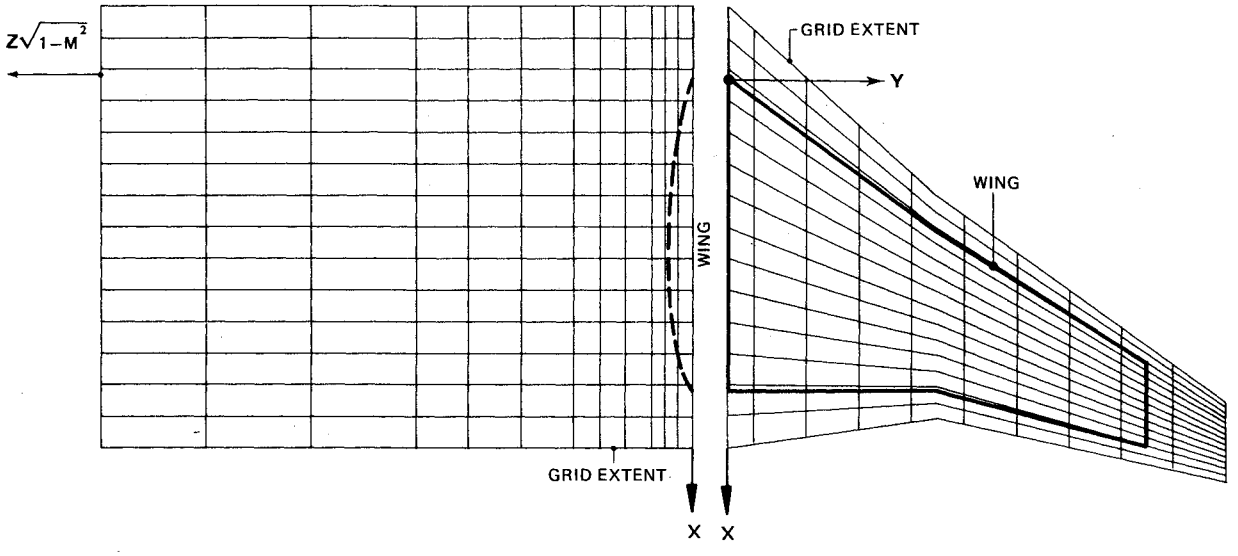

Fig. 2 Grid system in physical space.

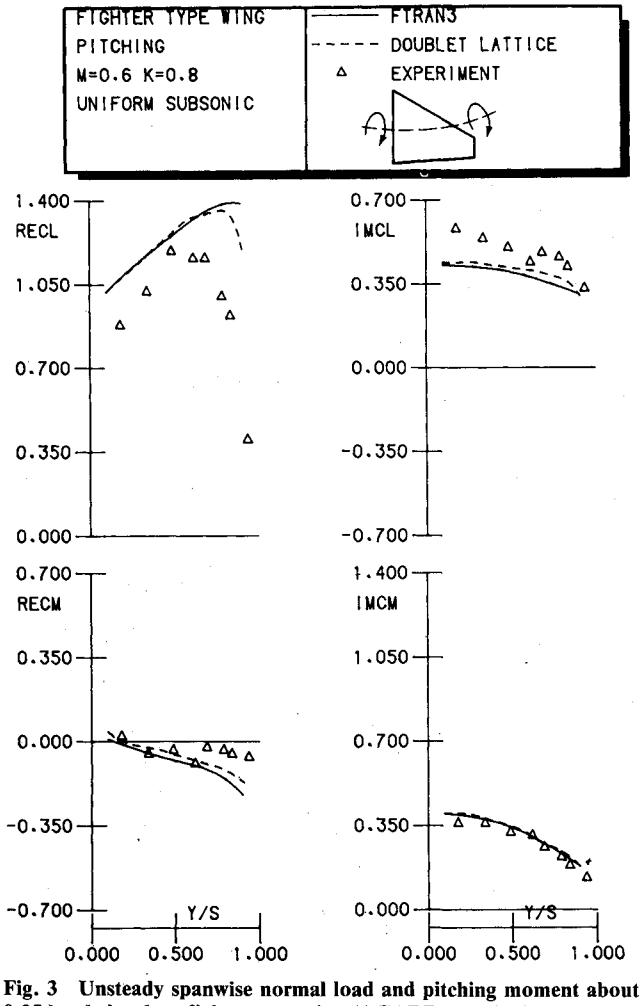

Fig. 3 Unsteady spanwise normal load and pitching moment about 0.25 local chord on fighter-type wing (AGARD notation) at subsonic conditions.

where L_f is the governing field (boundary) equation operator discretized on the fine grid and n denotes the iteration index.

2) Improvement of the current approximation φ^n on the fine grid by

$$\varphi^{n+\frac{1}{2}} = \varphi^n - S_f d_f^n$$

where S_f is a smoothing operator. The improvement depends on how close S_f approximates L_f^{-1} on the fine grid.

3) Calculation of defects on the coarse grid

$$d_c^n = RL_f\varphi^{n+\frac{1}{2}} + L_c\varphi_i^n - L_cR\varphi^{n+\frac{1}{2}}$$

where φ_i^n denotes the current integral approximation and L_c the governing field (boundary) equation operator discretized on the coarse grid.

4) Improvement of the current integral approximation φ_i^n by

$$\varphi_i^{n+1} = \varphi_i^n - S_cI_cd_c^n$$

where I is the integral (field panel) operator discretized on the coarse grid and S_c represents the coarse mesh smoothing operator which in subsonic flow regions can be chosen identically 1 because there I_c is a close approximate inversion of L_c [Eq. (2)]. In supersonic flow regions and at the wing boundary it is necessary to use a more implicit smoother.

5) Improvement of the current approximation $\varphi^{n+\frac{1}{2}}$ by

$$\varphi^{n+1} = \varphi^{n+\frac{1}{2}} + P(\varphi_i^{n+1} - R\varphi^{n+\frac{1}{2}})$$

6) $n=n+1$, go to item 1.

At convergence the algorithm will give

$$\varphi_1 = \varphi - PR\varphi \qquad \varphi_0 = PI_cH_c\varphi_i = PR\varphi$$

Computational Method FTRAN3

On the basis of the formulations given previously a computer code has been developed—FTRAN3. This section describes briefly the basic ingredients employed in FTRAN3.

Grid System

A stretched Cartesian grid is applied in the physical xz plane and a stretched sheared grid is used in the physical xy plane, see Fig. 2. The grid extends about a quarter-chord length from the leading and trailing edges in the x direction, about $2/(1-M^2)^{\frac{1}{2}}$ chord lengths from the wing in the z direction, and about one-quarter span length from the tip in the y direction. The coarse grid system is a restriction of the fine system chosen such that the default coarse mesh spacing is about three times the fine mesh spacing.

Difference Operators

The operators H_c, L_c, and L_f are obtained in conservative form using local geometric and fluid relations between the neighboring grid points (finite volume method[13,14]).

In supersonic flow areas artificial bias is introduced according to Ref. 15 to prevent unrealistic solutions and guarantee good performance of the relaxation-type smoothers.

Integral Operators

The integral or field panel operators are evaluated numerically as follows:

1) First a guess I_c^n is made using midpoint rule integration for all points except the sending point.

2) In regions where item 1 above is insufficient, I_c^n is improved by solving until accurate enough $H_c I_c = \mathfrak{X}$ [Eq. (2)] by the fast defect correction procedure:

$$I_c^{n+1} = I_c^n - I_c^n(H_c I_c^n - \mathfrak{X}) \tag{10}$$

where $\mathfrak{X}$ is the identity operator.

The first guess is accurate enough when the grid is rather uniform or when the distance between sending and receiving points is larger than the maximum grid spacing at the sending points. In the case first mentioned, Eq. (10) has to be applied only once for the sending point and then the evaluation is identical to that used in Ref. 8. In this way complicated algebraic forms and use of complicated integral rules are avoided.

Interpolation

Trilinear prolongation and weighted restriction are applied.

Smoothing

Line relaxation sweeps are performed on the fine grid in the x or z direction. The smoothing performance decreases as frequency increases. Thus far, in present applications the drop in performance is acceptable for the frequency range of interest. One can improve the performance by introducing frequency-related dissipation terms.

On the coarse grid point Jacobi relaxation is adopted in fluid regions where the Mach number differs slightly from the undisturbed Mach number. In other regions Crout factorization is applied in each x-z plane.

Boundary Conditions

Thus far, small-disturbance boundary conditions are applied on the mean wing plane ($z=0$). Also the pressures are calculated with the following small-disturbance formula:

$$Cp^l = -2(ik\varphi + \varphi_x) \tag{11}$$

In the future the small-disturbance boundary conditions and pressure representation will be replaced by the complete boundary conditions at the mean wing contour and the complete pressure formula. In order to accomplish the latter, a two-dimensional, time-linearized, full-potential code has been completed recently which is based on the same algorithm as used by the three-dimensional code. More details are presented in the last section concerning two-dimensional calculations.

Computational Performance

For computational efficiency and reliability a certain balance between the number of grid points on both grids should exist. The most important factor in the present two-level method is the coarse grid number N_c which gives the highest contribution $\mathcal{O}(N_c^2)$ to the overall computational cost. The fine grid gives a contribution of $\mathcal{O}(N_f)$, where N_f is the number of fine grid points. On the other hand, N_c has a strong influence on N_f and convergence; i.e., a decreasing N_c should lead to an increase of N_f and a decrease of the convergence speed for a given accuracy and the reverse.

At present a choice of $N_c = N_f/27$ seems to be optimal with which up to 20,000 fine grid points (i.e., 20,000 *complex* unknowns) can be treated in acceptable running times. It is NLR's opinion that this capacity will be sufficient for many transonic unsteady flow problems.

If, in the future, the capacity turns out to be too low (for example, due to an addition of a boundary-layer level) it can be increased and still have acceptable running times by: 1) reducing N_c and introducing a second or more finite difference level (or maybe a spectral method level) which does not contribute to the potential at A, or 2) introducing a second or more integral level to be treated efficiently with the cost reduction methods of Refs. 9 and 10.

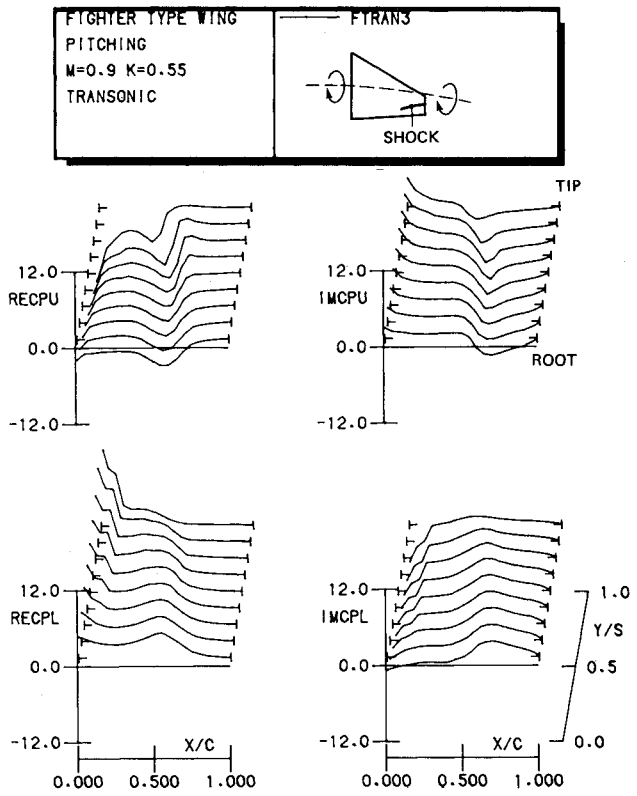

Fig. 4 First-harmonic pressure distributions on fighter-type wing at transonic conditions.

Convergence Strategy

A fixed strategy is used. First, the coarse level equations are solved until the trailing- and leading-edge potential changes are within a specified truncation error. Next, the multigrid method is used until the leading- and trailing-edge potential changes are within a specified truncation error. Usually it takes about 10 iterations to obtain three significant digits and reduce the maximum residual error two orders of magnitude.

Calculations

Calculations of oscillatory wing loads and pressure for planar configurations for various reduced frequencies and Mach numbers are performed to demonstrate the applicability of the present computational method FTRAN3.

Three types of results are shown:

1) Results obtained during the development of the computer code, where a Nφrstrud-type[16] approximation was used for the mean steady flowfield and the program was run consistently in a small-disturbance mode

$$(\Phi_{0_y} = \Phi_{0_z} = 0)$$

2) Results obtained recently where the mean steady flowfield has been obtained with the XFLO22-NLR code.[17]

3) Two-dimensional results.

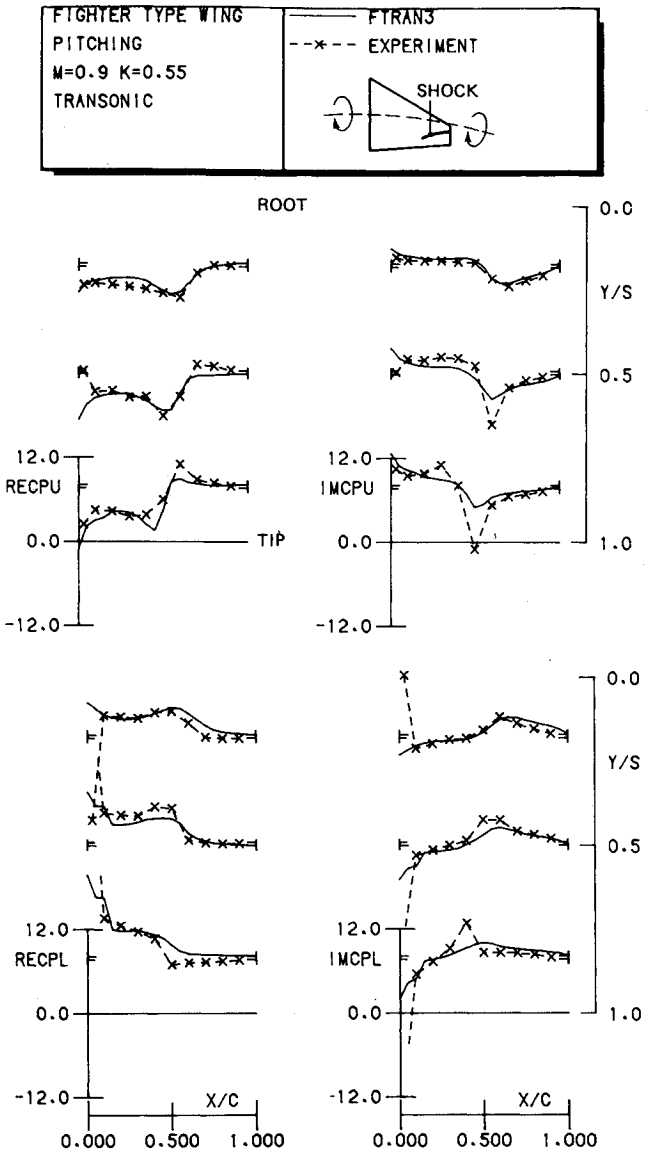

Fig. 5 Comparison of experimental and calculated first-harmonic pressures on fighter-type wing at transonic conditions.

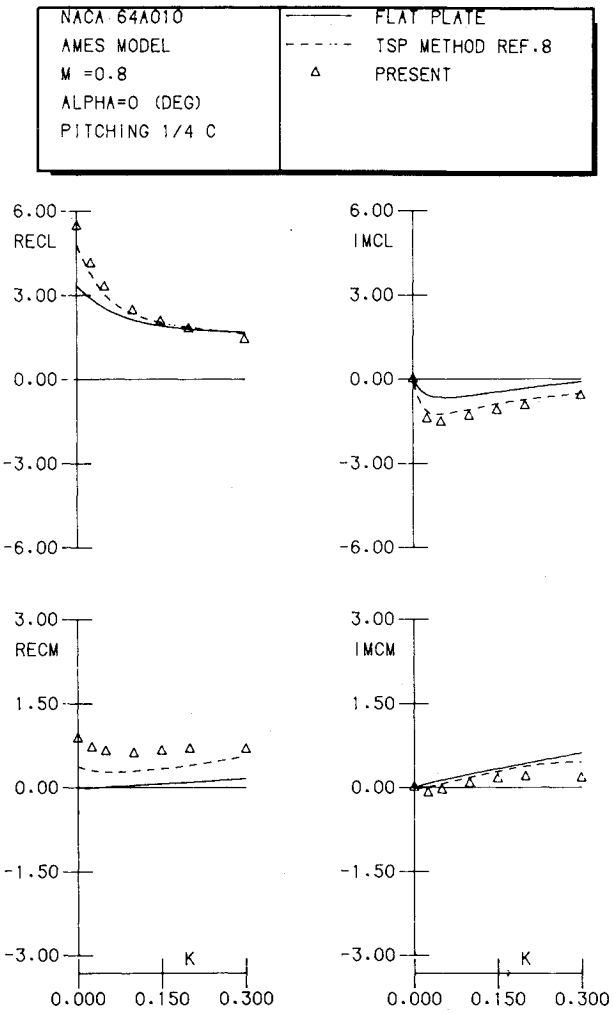

Fig. 6 Unsteady spanwise normal load and pitching moment about 0.25 local chord on fighter-type wing at transonic conditions (AGARD notation).

Results with an Approximated Mean Steady Flowfield

Calculations have been made for fighter- and transport-type wings where the mean steady flowfields have been obtained from the measured pressure distributions by an exponential decay in the vertical direction, originally introduced by Nφrstrud.[16] From the results it is hardly possible to draw conclusions about the quantitative performance of the method. They mainly serve as a measure for computational performance and give qualitative insight. In the near future results also will be available for which the steady flowfields have been calculated.

Fighter-Type Wing†

Calculations and comparisons have been made for pitching about the root midchord at two conditions: subsonic $M=0.6$, $k=0.8$; transonic $M=0.9$, $k=0.55$.

Subsonic Case (Uniform Mean Flow)

Figure 3 shows a comparison of the spanwise sectional loads distributions (AGARD notation) for results of the present method using a uniform mean steady flowfield (50 mesh points on wing upper and lower sides), the NLR doublet-lattice method (126 panels), and experimental data.[18]

The agreement between the theories is satisfactory. The differences at the tip are due to the insufficient grid spacing used by the FTRAN3 code. The experimental data have been included here as a reference of the differences that could be expected between theory and experiment at the transonic condition.

Transonic Case

A perspective view of calculated first-harmonic pressures at the upper and lower sides of the wing surface is shown in Fig. 4. Clearly visible are the pressure rises and falls due to the nonuniform Mach number distribution. Figure 5 shows a comparison of calculated and measured first-harmonic pressures at selected span stations. Except for peak values, a satisfactory agreement is shown. The spanwise sectional loads distributions are presented in Fig. 6. Comparisons are made between transonic and uniform subsonic FTRAN3 results and with the experiment. The transonic lift values are slightly different from the subsonic lift values. The differences are more pronounced between the moment values. As compared with Fig. 3 larger differences exist between theory and experiment. Part of the difference is probably due to the added complication of peak measuring and integration in the experiment. The computational time for the transonic case using $12\times20\times28$ grid points is about 2 min on the Cyber 170-855.

†Reference length is root chord.

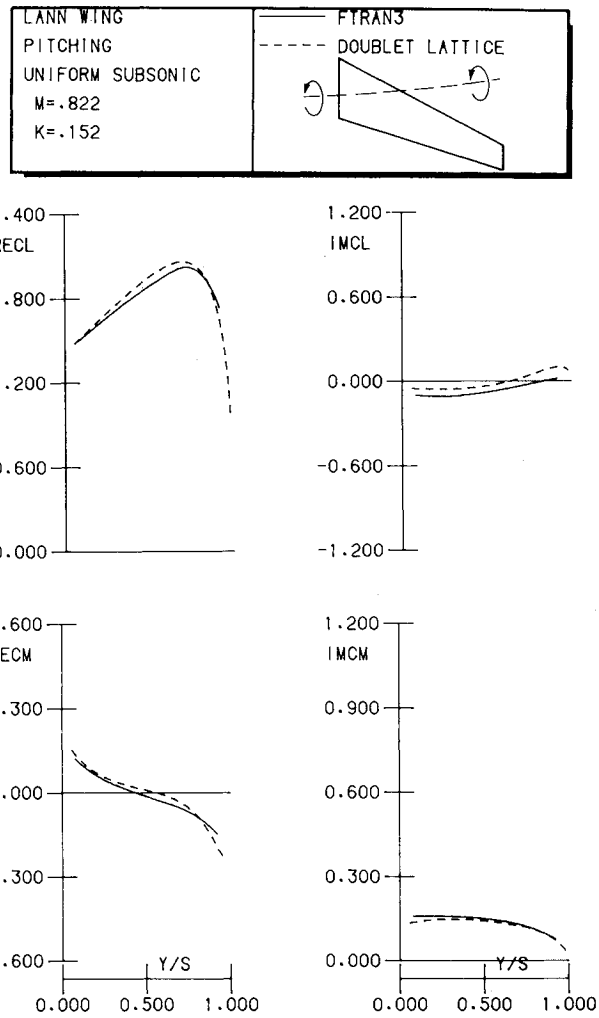

Fig. 7 Unsteady spanwise normal load and pitching moment about 0.25 local chord on transport-type wing at subsonic conditions (AGARD notation).

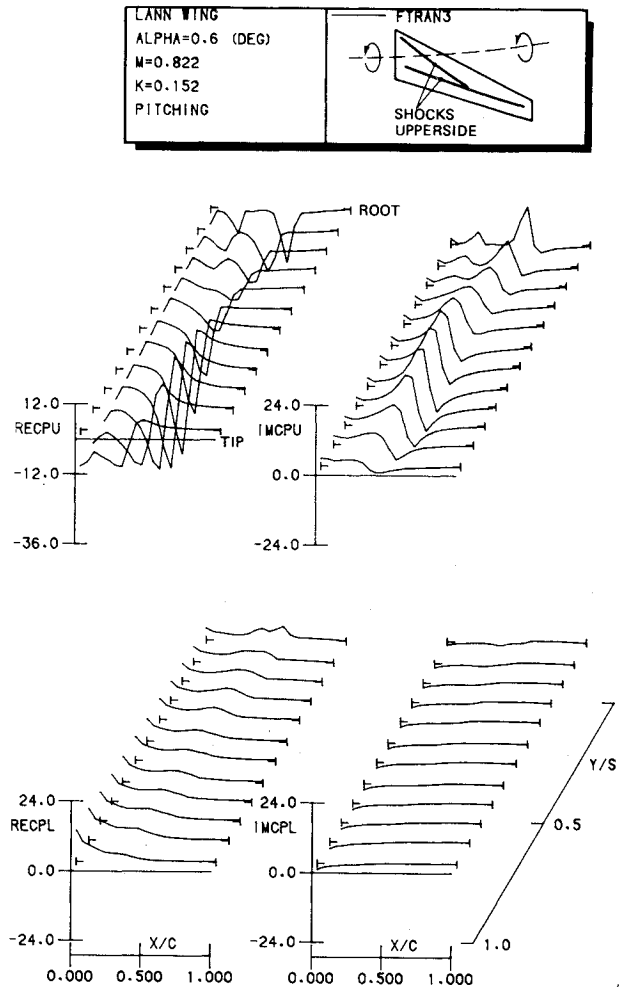

Fig. 8 First-harmonic pressure distributions on transport-type wing at transonic conditions.

LANN Transport-Type Wing‡

Calculations and comparisons were also made for the LANN wing, pitching about 0.621 root chord at $M=0.822$, $\alpha=0.6$ deg, and $k=0.152$.

Subsonic Case (Uniform Mean Flow)

The spanwise sectional loads distributions are compared to the present method (60 grid points on wing upper and lower sides) with the NLR doublet-lattice method (200 points on wing surface) in Fig. 7. The agreement is satisfactory. The differences are attributed to differences in mesh spacing.

Transonic Case

Figure 8 shows a perspective view of calculated first-harmonic pressures at the upper and lower sides of the wing surface. The lower side shows, except at the root, a rather subsonic distribution. The upper side clearly shows the effect of the lambda shock waves. Figure 9 shows a comparison of calculated and measured[19] first-harmonic pressures at selected span stations. A satisfactory agreement is shown here also, except for peak values. The spanwise sectional loads distributions are depicted in Fig. 10. Results of the present method are compared with the doublet-lattice method, the NLR quasi-three-dimensional method,[20] and the experiment. Large transonic effects and large differences between the results are shown. Part of the differences between the transonic methods and the experiment should be attributed here also to the added complication of peak measuring and integration in the experiment. The computation time for this case was also about 2 min on the Cyber 170-855 using $15\times20\times28$ grid points.

Results with a Mean Steady Flowfield Calculated with XFLO22-NLR

Calculations have been made for the ONERA M-6 (root chord reference length) wing at $M=0.84$ and $\alpha=3.06$ deg. The steady flowfield has been obtained by the XFLO22-NLR code and trilinearly interpolated from the XFLO22-NLR mesh system to the mesh system utilized by the FTRAN3 code. The unsteady calculation was performed for a pitching motion about the root midchord at a reduced frequency of 0.6 using the full-potential option with small-disturbance boundary conditions and pressure representation. Figure 11 shows a comparison of results of FTRAN3, and Ref. 5 for first-harmonic pressures on the upper side at selected span stations. A reasonable agreement is shown. Differences are shown clearly at the leading edge and at the peak caused by the motions of the shock waves. At the leading edge the results of FTRAN3 are affected more by the forward shock. A part of the difference is due to the small-disturbance boundary conditions, the pressure formula, and differences in steady flowfield. Another part could be explained by the differences between "time-integrating" and "time-linearized" methods. In the latter method it is implicitly assumed that the amplitude of oscillation is chosen such that the shock wave travels less

‡Reference length is mean aerodynamic chord.

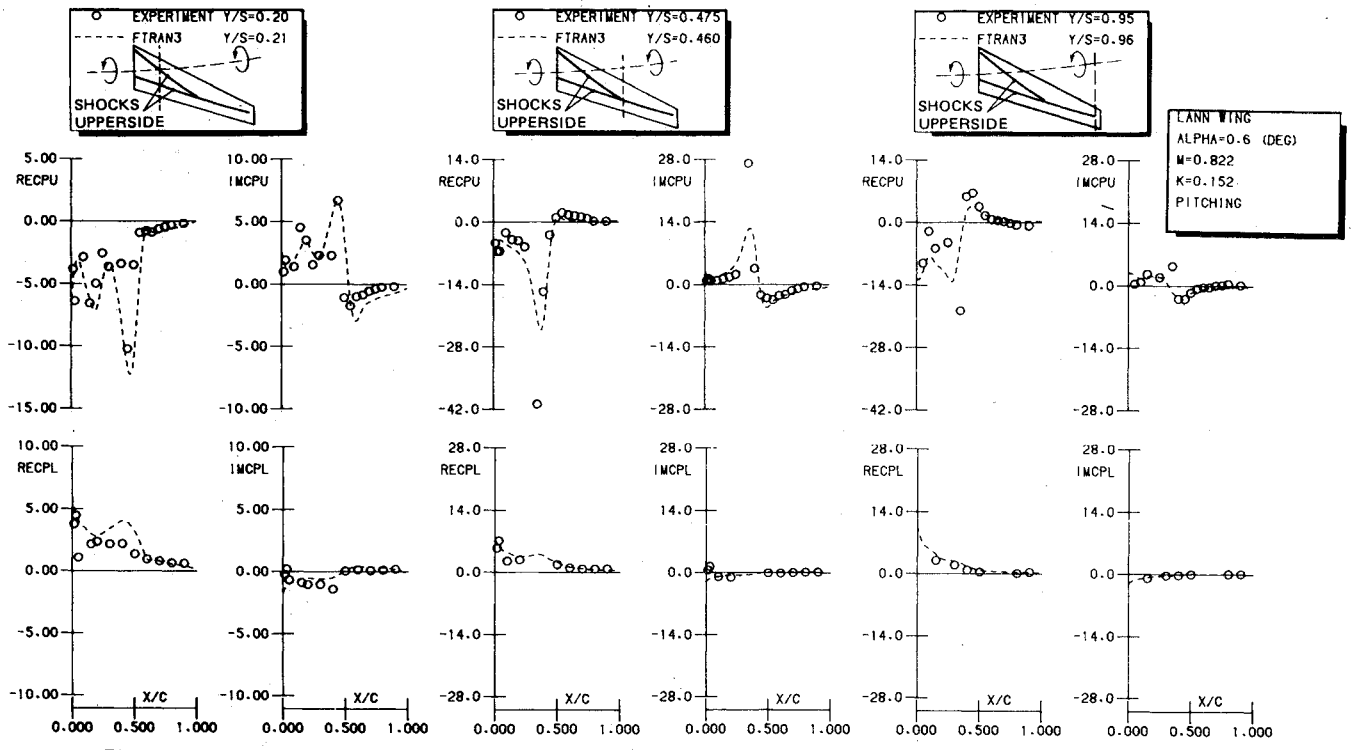

Fig. 9 Comparisons of experimental and calculated first-harmonic pressures on transport-type wing at transonic conditions.

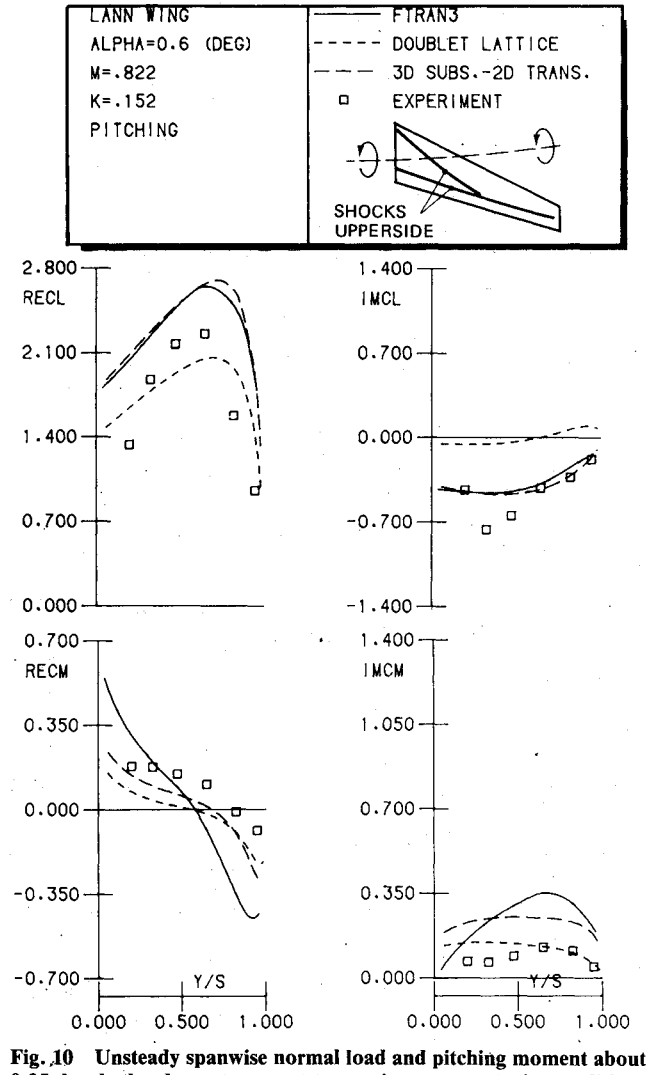

Fig. 10 Unsteady spanwise normal load and pitching moment about 0.25 local chord on transport-type wing at transonic conditions (AGARD notation).

than one mesh width. As a consequence, differences between peak width and peak height may exist. The computational time for this case was about 3 min on the Cyber 170-855 using $12\times20\times28$ grid points.

Two-Dimensional, Time-Linearized, Full-Potential Calculations

Recently a two-dimensional, time-linearized, full-potential code was completed based on the same algorithm as used by the three-dimensional code. The code utilized a body-fitted sheared rectilinear mesh system (H-type) and applies the complete boundary conditions and pressure representation. This two-dimensional code was developed primarily to investigate the implementation of boundary conditions at the mean wing contour and the use of the complete pressure representation. The steady potentials are obtained by the same algorithm which is embedded in a Newton procedure to account for the nonlinearity.

Results are obtained for the NACA 64A010 (Ames) airfoil at $M=0.8$, $\alpha=0$ deg on a 26×36 mesh system. The steady case needed about 30 iterations to reduce the maximum residual error three orders of magnitude. The unsteady cases needed also about 30 iterations. The slower convergence as compared with the three-dimensional cases is due to very large aspect ratios of the grid cells in the applied grid system together with the use of line relaxation in only one direction. [Application of the algorithm to a lifting flat plate ($k=0$) using an equidistant mesh system needed seven iterations and shows an error of 0.3% in C_{L_α}.]

Figure 12 compares the steady pressure distributions obtained with the present method and the transonic small perturbation (TSP) method of Ref. 1. Differences that could be expected show up at the leading and trailing edges and at the shock. Figure 13 compares unsteady lift and moment coefficients of calculations (AGARD notation[21]) with the present two-dimensional method, the two-dimensional TSP method described in Ref. 8, and flat-plate results.

As compared with flat-plate results, the coefficients exhibit a large difference. At reduced frequencies approaching zero, less agreement is found for the lift predicted by the transonic codes. The moments predicted by the transonic codes differ substantially over the entire frequency range. A part of those

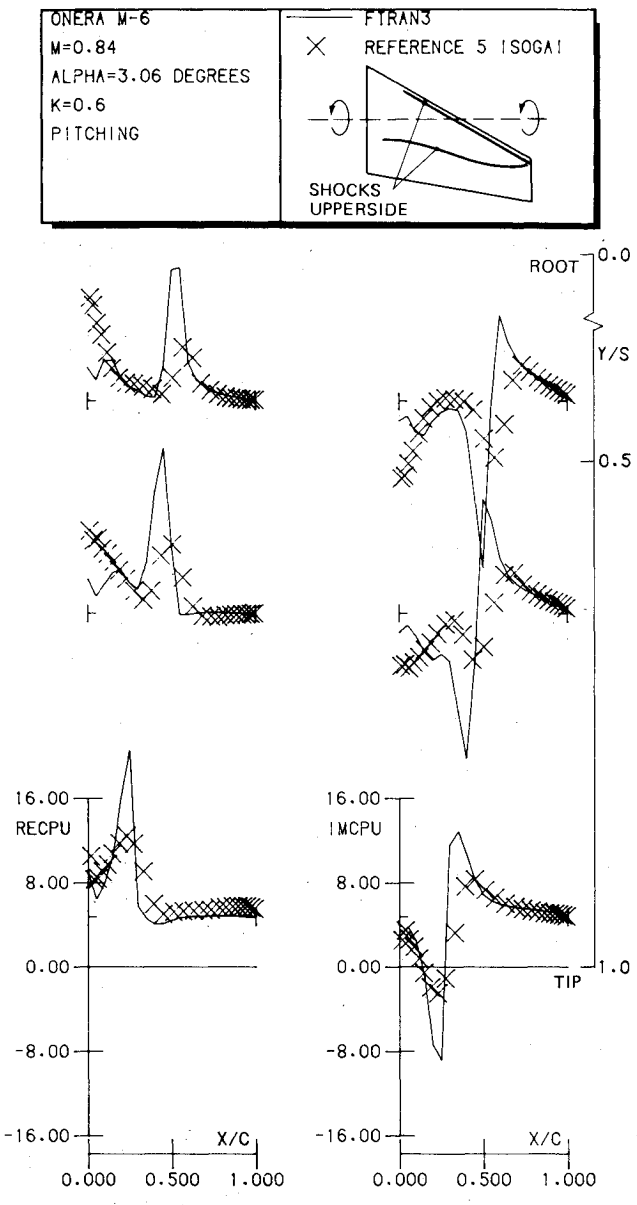

Fig. 11 Comparison of calculated first-harmonic pressures at the upper side of the Onera M-6 wing.

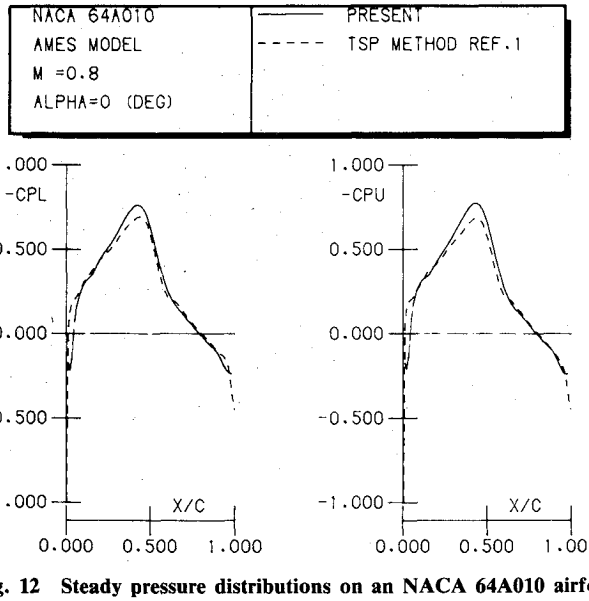

Fig. 12 Steady pressure distributions on an NACA 64A010 airfoil (Ames model).

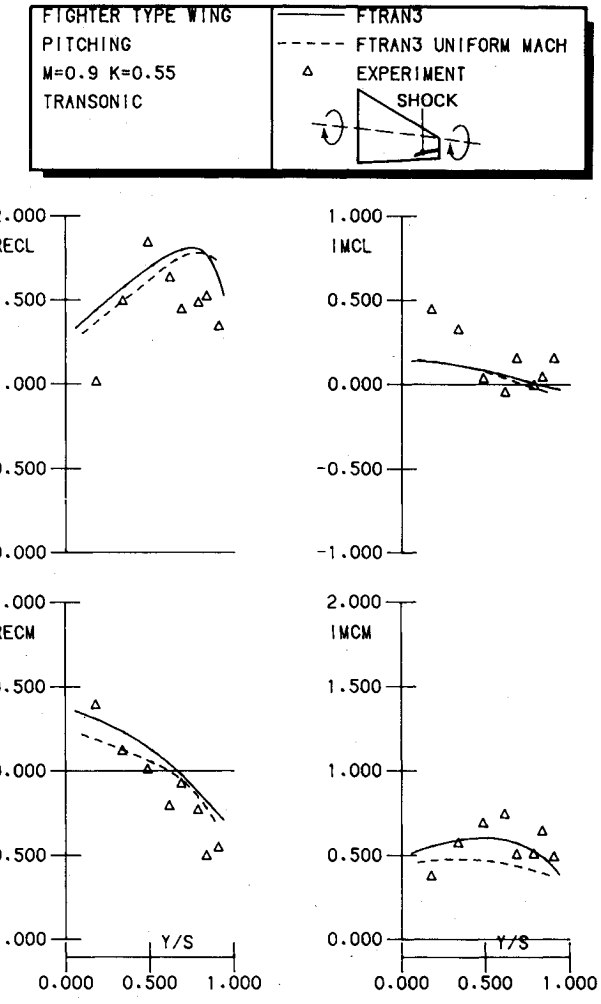

Fig. 13 Unsteady airloads on a pitching NACA 64A010 airfoil (AGARD notation).

differences is probably due to the differences between the steady flowfields.

Conclusions

A hybrid method which combines the advantages of finite difference and integral methods is presented for the calculation of "time-linearized," unsteady, transonic potential flows. The method is a mixture of recent developments in transonic calculation methods, particularly 1) the multigrid iterative approach for fast convergence, and 2) substantial reduction of grid points due to integral formulations. Grid generation is facilitated as well.

Unsteady three-dimensional applications of the present computer code FTRAN3 yielded the following conclusions:

1) Calculated results show satisfactory agreement with experimental data.

2) Calculated results compare reasonably well with Isogai's[5] time-integrating method.

3) The computational cost is low enough for routine flutter applications (about 4 × doublet lattice).

Acknowledgments

This investigation was carried out under contract for the Scientific Research Division of the Directorate of Materiel, Royal Netherlands Airforce (RNLAF). Special thanks are due to Mr. J. Th. van der Kolk of the Computational Aerodynamic Department for providing the link with the XFLO22-NLR system.

References

[1]Vooren, J. van der and Huizing, G. H., "Modified Version of LTRAN2: A Calculation Method for Inviscid Transonic Flow about Thin Airfoils in Moderately Slow Unsteady Motion," NLR TR 80059 L, June 1980.

[2]Isogai, K., "Numerical Study of Transonic Flutter for a Two-Dimensional Airfoil," NAL TR-617T, July 1980.

[3]Borland, C. J., Rizetta, D. P., and Yoshihara, H., "Numerical Solution of Three-Dimensional Unsteady Transonic Flow Over Swept Wings," AIAA Paper 80-1369, July 1980.

[4]Mulak, P., Gouston, M., and Angelini, J. J., "Extension of the Transonic Perturbation Approach to Three-Dimensional Problems," *Collected Papers of the International Symposium on Aeroelasticity*, Nuremberg, FRG, DGLR-Bericht 82-01, Oct. 1981, pp. 43-53.

[5]Isogai, K., "Calculation of Unsteady Transonic Potential Flow over Oscillating Three Dimensional Wings," NAL TR-706T, March 1982.

[6]Bridgeman, J. O., Steger, J. L., and Caradonna, F. X., "A Conservative Finite Difference Algorithm for the Unsteady Transonic Potential Equation in Generalized Coordinates," AIAA Paper 82-1388, Aug. 1982.

[7]Guruswamy, P. and Goorjian, P. M., "Comparisons between Computations and Experimental Data in Unsteady Three-Dimensional Transonic Aerodynamics, Including Aeroelastic Applications," AIAA Paper 82-0690, 1982.

[8]Hounjet, M.H.L., "A Field Panel Method for the Calculation of Inviscid Transonic Flow about Thin Oscillating Airfoils with Shocks," *Collected Papers of the International Symposium on Aeroelasticity,* Nuremberg, FRG, DGLR-Bericht 82-01, Oct. 1981, pp. 81-92.

[9]Hounjet, M.H.L., "Calculation of Unsteady Transonic Flows with Shocks by Field Panel Methods," *AIAA Journal*, Vol. 20, June 1982, pp. 857-859.

[10]Slooff, J. W., "Some New Developments in Exact Integral Equation Formulations for Sub- or Transonic Potential Flow," NLR MP 82024 U, May 1982.

[11]Albano, E. and Rodden, W. P., "A Doublet Lattice Method for Calculating Lift Distributions on Oscillating Wings in Subsonic Flow," *AIAA Journal*, Vol. 7, Feb. 1969, pp. 279-285.

[12]Brandt, A. and Dinar, N., "Multigrid Solutions to Elliptic Flow Problems," *Numerical Methods for PDEs, Proceedings of Symposium*, Mathematics Research Center, University of Wisconsin, Vol. 42, 1978, pp. 53-149.

[13]Jameson, A. and Caughey, D. A., "A Finite Volume Method for Transonic Potential Flow Calculations," AIAA Paper 77-635, June 1977.

[14]Caughey, D. A. and Jameson, A., "Progress in Finite Volume Calculations for Wing-Fuselage Combinations," *AIAA Journal*, Vol. 18, Nov. 1980, pp. 1281-1288.

[15]Boerstoel, J. W., "A Multi-Grid Algorithm for Steady Transonic Potential Flows around Airfoils using Newton Iteration," NLR MP 81050 U, Oct. 1981.

[16]Nørstrud, H., "Transonic Flow Past Lifting Wings," *AIAA Journal*, Vol. 11, May 1973, p. 754.

[17]Vooren, J. van der, Kolk, J. Th. van der, and Slooff, J. W., "A System for the Numerical Simulation of Sub- and Transonic Viscous Attached Flows around Wing-Body Configurations," NLR MP 82019 U, April 1982; also AIAA Paper 82-0935, June 1982.

[18]Tijdeman, H. et al., "Transonic Wind-Tunnel Tests on an Oscillating Wing with External Store," NLR TR 78106 U, Pt. II, Sept. 1978.

[19]Horsten, J. J., Boer, R. G. den, and Zwaan, R. J., "Unsteady Transonic Pressure Measurements on a Semi-Span Wind-Tunnel Model of a Transport-Type Supercritical Wing (LANN Model)," NLR TR 82069 U, Pts. I and II, July 1982.

[20]Steiginga, A and Houwink, R., "Correlation of Experimental and Quasi-3-D Theoretical Airloads on the Oscillating LANN Supercritical Wing Model," NLR TR 83003 U, Jan. 1983.

[21]*AGARD Manual on Aeroelasticity*, Vol. VI, 1971.